Evaluation of fracture toughness by small-punch testing techniques using sharp notched specimens

Jang-Bog Ju[a],[*], Jae-il Jang[b], Dongil Kwon[a]

[a]School of Materials Science and Engineering, Seoul National University, Seoul 151-742, South Korea
[b]Research and Development Division, Frontics Inc., Seoul 151-060, South Korea

Abstract

The small punch (SP) testing method has been used to assess the reliability of industrial facilities such as fusion reactor structures and power-generation systems. Conventional SP tests have evaluated flow properties, transition temperature, fracture strain, and other mechanical properties by analyzing load-deflection curves. However, previous research has not used a fracture-mechanics approach that considers flaws, stress analysis and fracture toughness. In this study, in order to obtain the fracture toughness based on fracture mechanics by SP tests, a sharp notch was machined into the central part of the SP specimens. A stress-intensity factor for sharp-notched SP specimens is proposed from analysis of stress fields near the crack tip. The crack initiation point was determined by analysis of the load-deflection curves combined with acoustic emission signals. The fracture toughness of SA 508 Class 3 steel was successfully evaluated by using the load at the crack initiation point.
© 2003 Elsevier Science Ltd. All rights reserved.

Keywords: Small punch test; Sharp notch; Stress intensity factor; Crack initiation point; Fracture toughness; Linear elastic fracture mechanics

1. Introduction

Many nuclear power plant components are subjected to severe environments in which materials deteriorate by time-dependent degradation mechanisms [1]. Such material degradation leads to crack initiation and propagation and can, in severe cases, cause rapid or catastrophic failure once the crack reaches a critical size. To assure structural integrity, frequent in-service inspections for flaws must be made using the procedures specified in the ASME Boiler and Pressure Vessel Code, Section XI [2].

However, in many practical situations, standard testing programs requiring a significant volume of sample material cannot be applied. Thus, new assessment methods are necessary that can characterize the condition of in-service components from small samples. Moreover, because economic and social factors increasingly demand extension of the lifetimes of existing nuclear power plants, the new techniques are concerned with evaluating the residual

lifetime as well as assessing the degree of embrittlement, which is essential for safe and reliable prolonged operation.

The small-specimen technique, which is a semi-non-destructive technique, is quite compatible with the above purposes. Small-specimen techniques were originally developed to cope with the restriction in irradiation volume in the development of fusion reactor materials [3,4]. This technique has several advantages over conventional test methods: it reduces the radioactivity of the irradiated materials, occupies a smaller area in the test facility, and avoids gamma heating [3].

Among these small-specimen techniques, the small-punch (SP) test has been useful in estimating mechanical properties by consuming smaller volumes of material than other methods. Several attempts have been made to obtain uniaxial tensile properties such as 0.2% yield stress, tensile strength, and ductility by analyzing load-deflection data recorded during the SP test [5–8]. Baik et al. [5], studying the ductile-brittle transition temperature (DBTT) of reverse-temper-embrittled ferritic steel using the SP test, observed that the SP test showed well-defined ductile–brittle transition characteristics and demonstrated the relationship between the SP transition temperature and the conventional

* Corresponding author. Tel.: +82-2-880-8404; fax: +82-2-886-4847.
  E-mail address: jjbbb@snu.ac.kr (J.-B. Ju).

Charpy DBTT [9–13]. In ductile metals, fracture toughness was estimated in terms of SP test data in which an effective fracture strain was measured and empirically correlated with fracture toughness [10,14].

The present study aims at evaluating the fracture toughness of structural steels by the SP test. In a conventional SP test, fracture is assumed to occur at a maximum load that is correlated with fracture characteristics. However, experimental observations have shown that the crack initiates before the maximum load and propagates until final fracture occurs [13]. In this study, in order to overcome this problem and arrive at a valid fracture toughness based on fracture mechanics, a sharp notch is introduced into the SP specimen and the stress intensity factor, K, of the crack is obtained through analysis of the stress fields near the crack tip.

2. Theoretical analysis

Fracture mechanics methodology is based on the assumption that all engineering materials contain cracks from which failure starts. The estimation of the residual life of machine or structural components requires knowledge of the stress redistribution caused by the introduction of cracks in conjunction with a crack-growth condition. Cracks produce a large stress elevation around the crack tip that needs particular attention because further crack growth takes place at that point. Except in ideally brittle materials, loading of a cracked body is usually accompanied by inelastic deformation in the vicinity of the crack tip. In some situations, however, the extent of inelastic deformation is very small compared to the crack size and other characteristic lengths of the body, and elastic theory is adequate to address the stress distribution in the cracked body. Stress intensity factors have been applied to predict the static strength of cracked bodies and have also been shown to predict fracture behaviour and to control the rate of crack propagation under cyclic loading. In each case, the significant stresses in the crack tip vicinity are associated with a stress singularity of $(r)^{-1/2}$, where r is the radial distance from the crack tip.

To apply the concept of stress intensity factor to the SP test, the analysis by Sih et al. [15] for thin plate subjected to out-of-plane bending was adopted. Consider the SP test as the problem of an infinite plate containing a crack of length $2a$, where a bending force, M_0, is applied all around the plate boundary at infinity, as illustrated in Fig. 1. The resulting stress intensity factor has the form

$$K_1 = \frac{6M_0}{h^2} a^{1/2} \text{ and } K_2 = 0. \tag{1}$$

Upon observing that $6M_0/h^2$ is the stress on the surface layer of the plate at infinity, this result is similar to the 'corresponding' extensional problem, i.e. uniform extensional stress, σ, at infinity, which gives $K_I = \sigma a^{1/2}$.
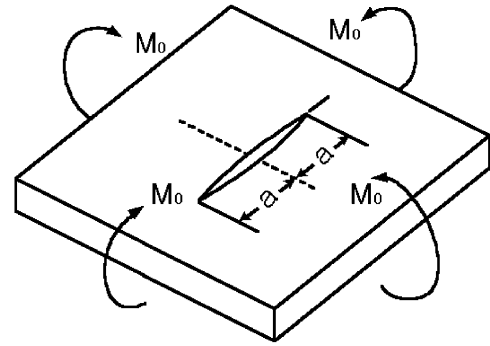

Fig. 1. Infinite plate containing crack and subjected to uniform bending.

To calculate the bending force on a SP specimen, we begin with the case in which the load is uniformly distributed along a circle of radius r (Fig. 2(a)) and consider separately the portion of the plate inside and outside this circle. For each portion, a general equation is used with a total stress $q = 0$ for both portions and total load $P = 0$ for the inner portion. The arbitrary constants are determined in such a way as to satisfy the continuity conditions on the circle $x = r$.

For the inner portion $(x < r)$:

$$w = \frac{P}{8\pi D}\left[-(x^2 + r^2)\ln\frac{c}{r} + (x^2 - r^2) + \frac{1}{2}\left(1 + \frac{r^2}{c^2}\right) \right.$$
$$\left. \times \left(c^2 - x^2\right) \right]. \tag{2a}$$

For the outer portion $(x > r)$:

$$w = \frac{P}{8\pi D}\left[-(x^2 + r^2)\ln\frac{c}{x} + \frac{1}{2}\left(1 + \frac{r^2}{c^2}\right)(c^2 - x^2) \right]. \tag{2b}$$
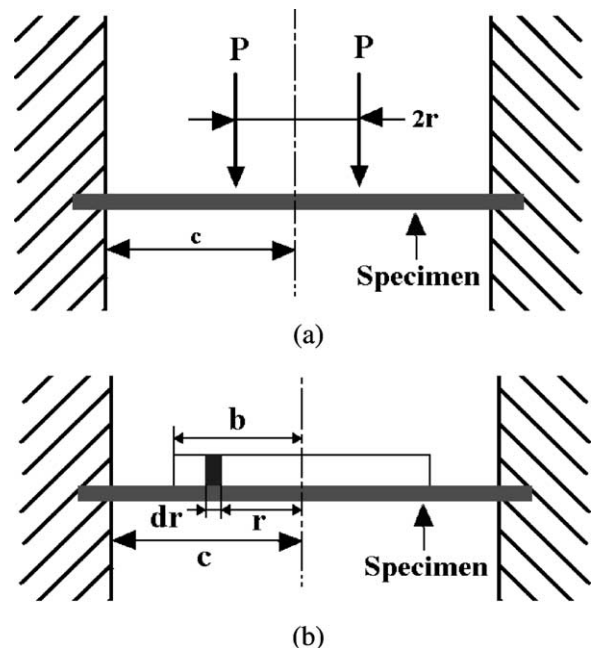

Fig. 2. Schematic diagrams of concentrically loaded circular plate.

Table 1
Chemical compositions of the materials used in this study (wt.%)

	C	Mn	Si	Al	Ni	Cr	Mo	P	S	Cu
SA 508-1	0.19	1.35	0.09	0.009	0.82	0.16	0.52	0.008	0.004	0.04
SA 508-2	0.20	1.42	0.07	0.005	0.79	0.15	0.57	0.007	0.003	0.06
SA 508-3	0.21	1.36	0.24	0.022	0.92	0.21	0.49	0.007	0.002	0.03

Any case related to the bending of a circular plate loaded symmetrically with respect to the centre can be solved by using these equations together with the method of super-position. Consider the case shown in Fig. 2(b) as a SP specimen in which the load is uniformly distributed over the inner part of the plate bounded by a circle of radius b. Substituting into Eq. (2a) yields $dP = 2\pi r q dr$, and the curvature produced at the centre by the entire load is then

$$\left(\frac{d^2w}{dx^2}\right)_{x=0} = \frac{q}{4D}\int_0^b\left(-2\ln\frac{c}{r}+1-\frac{r^2}{c^2}\right)r dr$$
$$= -\frac{qb^2}{4D}\left(\ln\frac{c}{b}+\frac{b^2}{4c^2}\right). \tag{3}$$

The corresponding bending force at the centre is

$$M_0 = -D(1+\nu)\frac{d^2w}{dx^2} = \frac{1+\nu}{4\pi}P\left(\ln\frac{c}{b}+\frac{b^2}{4c^2}\right) \tag{4}$$

where b and c are the contact radius and the lower die radius, respectively. The contact radius b continuously increases with increasing applied load and it is difficult to determine the value of b during punch loading. So, the results of Joo et al. [8] were used to represent the relationship between contact radius and applied load. The contact radius increases with applied load, but can be presented in master curves; by regression, the value of b was determined.

In order to obtain fracture toughness values based on fracture mechanics, the crack initiation point must be determined, and this was done here by using the change in shape of the curves. Thus, by substituting Eq. (4) into Eq. (1) and using the load at the crack initiation point (P_i), the fracture toughness of thin plate with a through-thickness

crack under a bending force was obtained as

$$K_C = \frac{3}{2}\frac{P_i(1+\nu)}{\pi h^2}\left(\ln\frac{c}{b}+\frac{b^2}{4c^2}\right)\sqrt{a}. \tag{5}$$

3. Experimental procedures

The materials used in this study were three kinds of the ASME SA 508 Class 3 steels generally used in Korea for nuclear reactor pressure vessels, denoted as SA 508-1, SA 508-2 and SA 508-3. Their chemical compositions are listed in Table 1.

SP specimens were of rectangular type with dimensions 10 by 10 mm by 0.5 mm, a specimen size frequently used because it can be machined easily from the undamaged part of a broken Charpy V-notch specimen. A through-thickness-type notch (1.0 mm length and 0.5 mm wide) was machined into the centre part of the SP specimen by wire cutting. Fig. 3 shows a SP specimen and the location and shape of the sharp notch. The crack tip radius is made as sharp as 20 μm. To adjust the thickness and eliminate the effects of surface roughness, both sides of the SP specimen were mechanically polished with up to 2000 emery paper. After ultrasonic cleaning, the crack shape and length were examined under an optical microscope.

The experimental apparatus for the SP test, shown in Fig. 4, consists basically of a puncher, a ball and dies. The specimen is supported on the lower die and fixed by four clamping screws between the upper and lower dies. As the load is applied to the specimen by the ball through the puncher, the specimen is displaced into the lower die. The clamping holder prevents specimens from cupping upwards during punching and therefore the deformation is concentrated in the region below the punch. A steel ball of
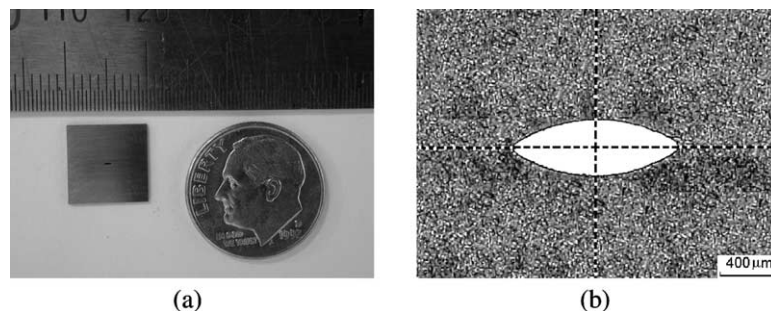

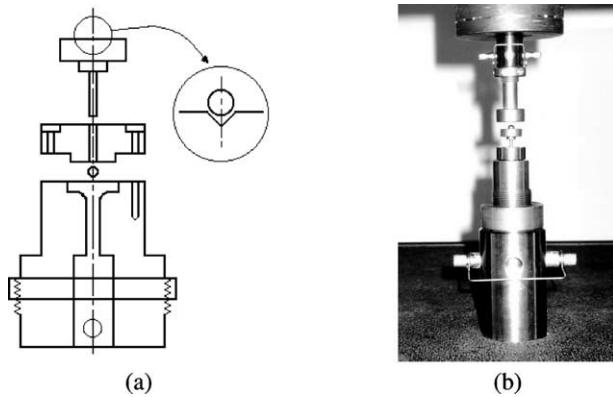Fig. 3. (a) Geometry of SP specimen and (b) shape and location of pre-crack.

Fig. 4. (a) Cross-section of loading configuration in SP test and (b) photograph.

2.4 mm diameter, with hardness more than HRC 50, is used to displace the SP specimen to prevent plastic deformation of the ball. According to previous investigation, the alignment of the punch, specimen and die axes limits the accuracy of data, since specimen stiffness increases with loading eccentricity [7]. Thus the testing apparatus used in this study is similar to that in other reports [3–7] except that another steel ball (4 mm diameter) was used for system alignment and load-line centering.

A universal tensile machine with a load cell of 5 kN capacity was used for the SP test. The specimen was punched under a constant punch displacement rate of 1.2 mm/min until a 10 percent or greater decrease in the peak load occurred. The test temperatures were liquid nitrogen (LN) temperature, 77 K, and room temperature, 298 K. For tests at LN temperature, the punch, specimen and die assembly were fully immersed in liquid nitrogen for specimen temperature control during punching and were tested only after at least 1 h. SP tests were performed on specimens with and without notches.

To determine the crack initiation point, an acoustic emission (AE) sensor was attached to the lower die of the testing apparatus, not to the specimen itself since it was too small for the sensor to be attached directly. The AE signal from the sensor system passed through a preamplifier with 40 dB gain and frequency response in the range 10 kHz–1 MHz. The AE signal was further amplified, conditioned with various filter bandwidths and processed as several AE parameters such as AE hits, AE energy, ring-down counts and RMS (root mean square) voltage.

Some of the tests were interrupted to examine the specimen for microcracking in the scanning electron microscope (SEM). SEM was also used as necessary to investigate fracture modes and crack extension.

4. Results and discussion

Fig. 5 shows load-deflection curves obtained at 298 K from SA 508 specimens without sharp notches. Because
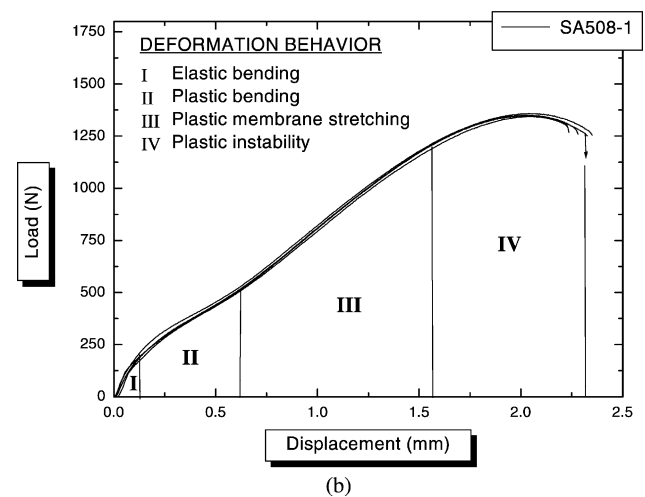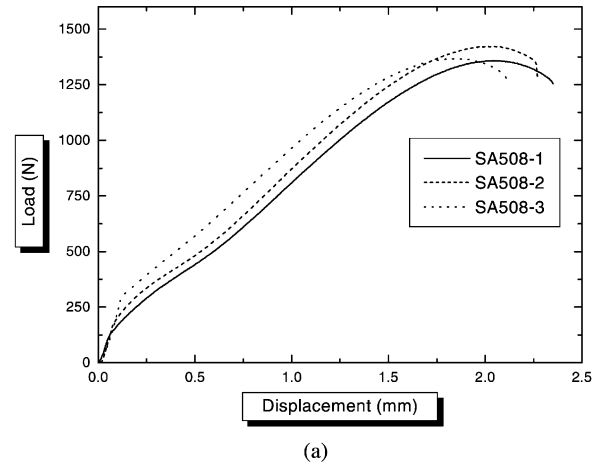

(a)

(b)

Fig. 5. Load-deflection curves of the specimen without pre-crack tested at room temperature.

the steel ball maintained the testing apparatus alignment, reproducible and repeatable results were obtained, as shown in Fig. 5(b). The nature of failure in a SP specimen changes with the temperature. At low temperature, early crack initiation and rapid crack growth within the plastic bending regime lead to brittle failure before the membrane stretching and plastic instability regimes are reached. Fig. 6 shows typical load-deflection curves of a SA 508-1 specimen with test temperature. At room temperature, the shape of load-deflection curve can be divided into four typical deformation regimes, as indicated in Fig. 5(b). But at LN temperature, the maximum load and the deflection decreased abruptly because of the change in yield strength with test temperature. The temperature dependence of load-deflection curves was accompanied by a change in fracture mode, as shown in Fig. 7. At room temperature, a long crack grew along the circumferential direction with substantial plastic deformation; cracking was ductile in nature (see Fig. 7(b)). At LN temperature, several radial cracks were observed and the depth of bulging deformation dramatically decreased with little change in thickness. These trends are consistent with various workers' observations [5–8].
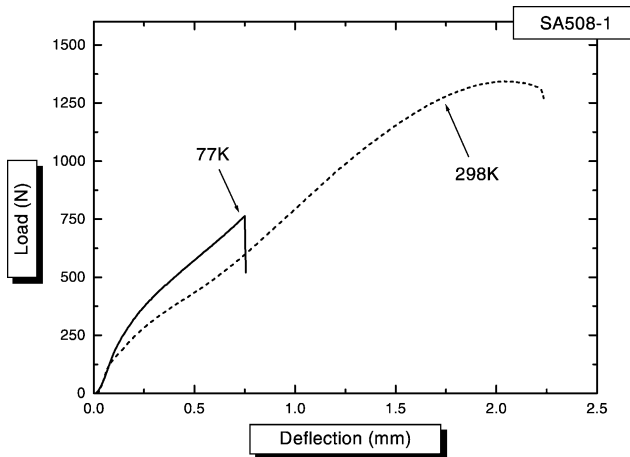
Fig. 6. Load-deflection curves obtained at different test temperatures.

Fig. 8(a) shows the load-deflection curve of a SA 508-1 specimen with a sharp notch. The maximum load and deflection up to maximum load of this specimen were both lower than for the specimen without the sharp notch, probably because of the loss of the ability to cover the full load due to the existence of the sharp notch. However, four deformation regimes were also observed, although they were somewhat different from those for the specimen without the sharp notch.

In order to obtain the fracture toughness based on fracture mechanics, the crack initiation point must be determined. In the upper shelf region, however, crack initiation cannot be detected from the load-deflection curve because its growth is ductile and gradual, as mentioned above. In this study, therefore, the AE signals were analyzed

for information about the deformation and fracture behaviour of the SP specimen during testing. AE is caused by the generation of high-frequency elastic waves accompanying plastic deformation and fracture in solids [16]. Variations in the emission characteristics are thought to result from the different mechanisms responsible for their generation, such as dislocation movement, void coalescence, crack initiation, and fracture. The AE energy, defined as the sum of the AE count occurring during one AE hit, and the load-deflection curve of a SA 508-1 specimen with a sharp notch are shown in Fig. 8. The AE energy peaks were observed in the initial region, the plastic-bending regime and the maximum-load region of the curve. The peaks in the initial region can be explained by slip-band formation during deformation [17] and those in the maximum-load region are due to the final fracture. Thus we conclude that the peaks of the plastic bending regime reflected crack growth and that the starting point of these peaks can be defined as the crack initiation point. In other words, the stable crack initiated in the plastic bending regime and propagated until final fracture occurred. We conducted the SP test at least five times. Though the magnitudes of AE energies were somewhat different for each test, we obtained reproducible results for the crack initiation point. Thus, we have used the average values.

In order to ascertain the crack initiation point, SEM photographs were taken of the cracked specimens at various points of the load-deflection curve, as shown in Fig. 9. After the slip-band peaks (Fig. 9(a)), there were no signs of notch extension. After the crack initiation and growth peaks (Fig. 9(b)), an extended crack was observed at the tip of the sharp notch. From these observations, we can conclude that the sharp notch played the role of a stress concentrator and
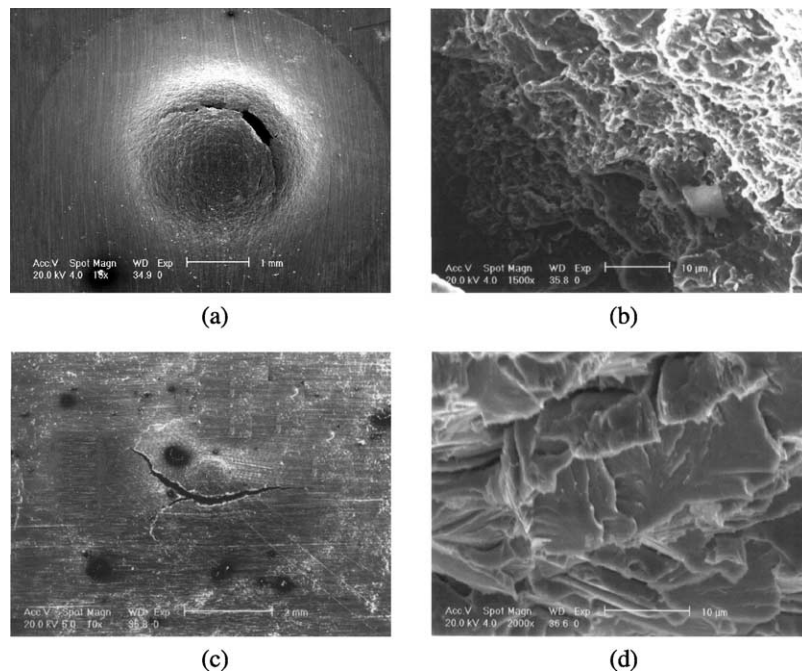

Fig. 7. SEM micrographs: crack shapes at (a) room temperature and (c) LN temperature, and their fractographs at (b) room temperature and (d) LN temperature.
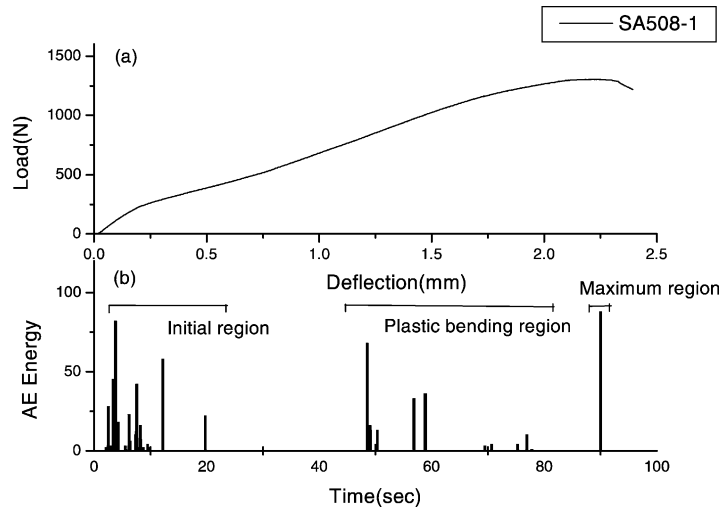
Fig. 8. (a) Load-deflection curve and (b) acoustic emission signals at room temperature for SA 508-1 specimen with pre-crack.
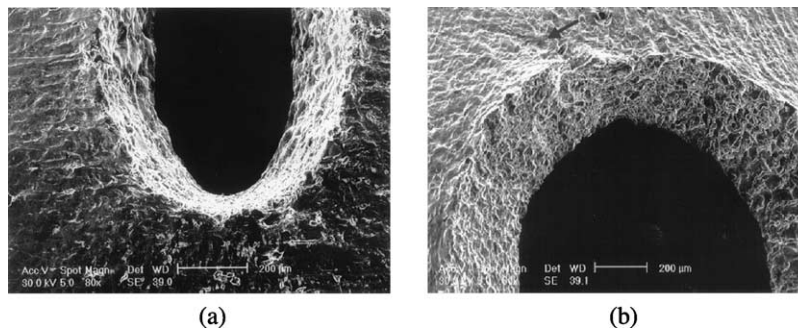

Fig. 9. SEM micrographs of cracked specimen after (a) initial peaks (at 0.7 mm deflection) and (b) crack initiation and growth peaks of AE signals (at 1.3 mm defelction). (Arrow in (b) indicates the extended crack.)

that the crack initiated at the sharp notch tip in the plastic bending regime. Thus the load at the first AE peak of the plastic bending regime was determined to be the crack initiation load.

Fig. 10 shows load-deflection curves for the specimens with sharp notches tested at LN temperature. Unfortunately, AE signals could not be obtained at LN temperatures because we failed to control and minimize the noise in the testing apparatus due to the LN coolant. The crack initiation point for the specimen tested at LN temperature was determined by the shape change in the load-deflection curves. Because fracture occurred in the elastic bending regime, the maximum load could be successfully used as the crack initiation load. Fig. 11 shows that the crack initiated at the tip of the sharp notch and extended away from the punch region, with little accompanying plastic deformation.

The fracture toughness values shown in Table 2 were evaluated by inserting the load at crack initiation into Eq. (5). Fracture toughness values obtained by our approach have little scatter and we used average values. The values are compared with those from the master curve for SA 508 steels in ASTM E1921 [18], which are also listed in Table 2. The master curve is proposed to determine the characteristic

temperature (T_0) representing fracture toughness in the transition range using a statistical probability model. The temperature dependency of fracture toughness represented by the master curve is:

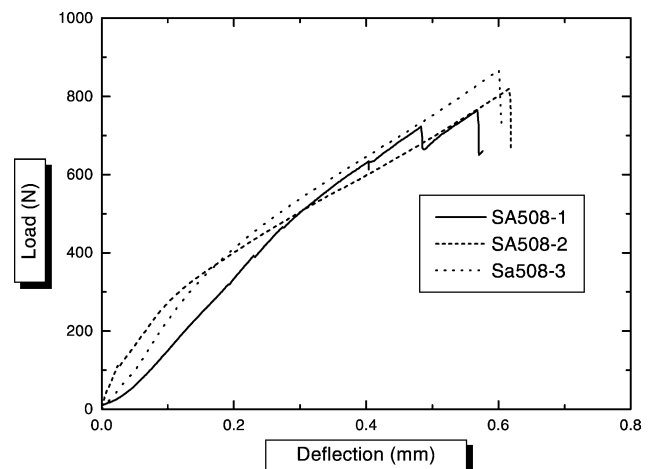$$K_{JC(med)} = 30 + 70e^{[0.019(T-T_0)]} \qquad (6)$$

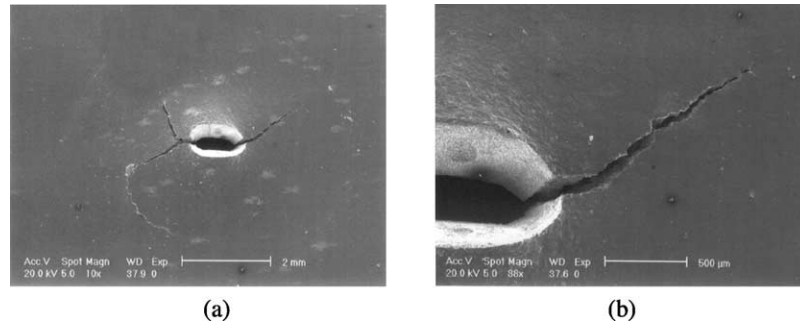Fig. 10. Load-deflection curves at LN temperature for specimen with pre-crack.

Fig. 11. SEM micrographs after tests showing brittle crack extension.

where $K_{JC(med)}$ is the average fracture toughness calculated from the master curve and T_0 is the temperature at which the fracture toughness of a 25 mm-thick specimen is 100 MPam$^{1/2}$. T_0 was determined from the precracked Charpy specimen tested under static loading [19] and is also listed in Table 2. Fracture toughness values calculated by the master-curve method are generally expressed with a 5% regression curve. The deviation error range is about 5 MPam$^{1/2}$ and 120 MPam$^{1/2}$ at LN and room temperature, respectively.

At LN temperature, our results were congruent with those of the standard testing methods. The reason for the somewhat higher toughness in the SP tests can be explained as follows. First of all, the sharp notches in this study have a relatively blunt tip due to the mechanical machining. An increase in the root radius at the crack tip could increase the fracture toughness, since fracture mechanics theory assumes an infinitely sharp crack. But such an effect can be ignored in this study, since the root radius of the sharp notch did not exceed 20 μm and many workers report that fracture toughness is unrelated to the root radius below several tens of μm [20,21]. Another explanation would be the thickness effect. Conventional fracture toughness tests must satisfy the specimen size requirement. Since small thickness corresponds to a nominally plane stress condition and fracture toughness increases with decreasing thickness, this thickness effect results in a little higher toughness in our SP test [22]. This is consistent with the fact that total strain in a conventional SP test decreases with increasing thickness [7].

The fracture toughness values in the SP test are much lower at room temperature than those on the master curve. At room temperature, fracture toughness values on the master curve include substantial plastic deformation. For the SP test results in Fig. 9, even though the crack initiated at the tip of the sharp notch, plastic deformation and gradual extension of the crack followed. However, the fracture toughness in the SP test in this study was based only on linear elastic fracture mechanics, which yields a lower toughness. Hence, considering plastic deformation and crack growth, a parameter reflecting SP energy (defined as the area under the load-deflection curve until final fracture) can be suggested as a useful tool for calculating the J integral [23]. The present authors will consider these issues in future work.

The present results suggest that, if further research on such issues as sharp notch shape and thickness effect is successful, the linear elastic fracture toughness obtained in a SP test with a sharp notched specimen could be successfully applied in nuclear facilities and on many in-service components.

5. Conclusions

Small punch tests were performed on a class of materials used in nuclear pressure vessels in order to assess fracture toughness and thus evaluate the remaining life of components.

Experimental reproducibility was obtained in our small punch testing systems by using a steel ball for alignment. The small punch test exhibited a temperature dependence associated with cleavage fracture at low temperature and ductile fracture at high temperature. In order to extract fracture mechanics information from the small punch specimen, a through-thickness-type sharp notch was introduced at its centre to play the role of a stress concentrator.

The stress intensity factor of the sharp-notched small punch specimen was determined from analysis of the stress fields near the crack tip using a complex-variable method. By using the load at the crack initiation point, which was determined from the analysis of acoustic emission signals and load-deflection curves, the fracture toughness of the small punch test was expressed as:

Table 2
Fracture toughness values obtained by SP tests and ASTM E1921 master curves method (MPam$^{1/2}$)

	SP TEST		MASTER CURVE		
	77K	298K	77K	298K	T_0 (°C)
SA 508-1	38.19	57.03	35.75	245.96	−64.5
SA 508-2	35.03	52.55	33.61	243.99	−40.0
SA 508-3	41.02	59.43	37.02	249.21	−75.0

$$K_C = \frac{3}{2} \frac{P_i(1+\nu)}{\pi h^2} \left(\ln \frac{c}{b} + \frac{b^2}{4c^2} \right) \sqrt{a}$$

The fracture toughness of SA 508 Class 3 nuclear pressure vessel steels was evaluated using the above equation and was compared with those from the master curve suggested in ASTM E1921. In the lower shelf energy region (77 K), congruent results were found, and our fracture toughness formula will be used in further life-assessment calculations. These results demonstrated the feasibility of using the small punch test to extract the fracture toughness based on fracture mechanics on many in-service components.

References

[1] Shah VN, MacDonald PE. Aging and life extension of major LWR components. Netherlands: Elsevier; 1993.

[2] ASME boiler and pressure vessel code Section XI; 1989.

[3] Lucas GE. Review of small specimen test techniques for irradiation testing. Metall Trans A 1990;21A:1105–19.

[4] Jung P, Hishinuma A, Lucas GE, Ullmaier H. Recommended miniaturized techniques for mechanical testing of fusion materials in an intense neutron source. J Nucl Mater 1996;232:186–205.

[5] Baik J-M, Kameda J, Buck O. The use of small-scale specimens for testing irradiated material. ASTM STP 888. Philadelphia: American Society for Testing and Materials; 1986.

[6] Fleury E, Ha JS. Small punch tests to estimate the mechanical properties of steels for steam power plant: I. Mechanical strength. Int J Pressure Vessels Piping 1998;75:699–706.

[7] Cheon JS, Kim IS. Initial deformation during small punch testing. J Test Eval 1996;24(4):255–62.

[8] Joo Y-H, Hashida T, Takahashi H, Shimomura K. The use of small punch (bulge) tests to estimate fracture stress in the lower shelf regime. J Test Eval 1992;20(5):336–42.

[9] Baik J-M, Kameda J, Buck O. Small punch test evaluation of intergranular embrittlement of an alloy steel. Scripta Metallurgica et Materialia 1983;17:1443–7.

[10] Kameda J, Mao X. Small-punch and TEM-disc testing techniques and their application to characterization of radiation damage. J Mater Sci 1992;27:983–9.

[11] Tokitsu K, Joo Y-H, Nei T, Shimomura K, Hashida T, Takahashi H. Development of dynamic small punch testing method and prediction of the ductile-brittle transition temperature. Trans Japan Soc Mech Eng A 1991;57(544):2911–5.

[12] Kameda J, Buck O. Evaluation of the ductile-to-brittle transition temperature shift due to temper embrittlement and neutron irradiation by means of a small-punch test. Mater Sci Eng 1986; 83:29–38.

[13] Foulds J, Viswanathan R. Small punch testing for determining the material toughness of low alloy steel components in service. J Eng Mater Tech 1994;116:457–64.

[14] Mao X, Shoji T, Takahashi H. Characterization of fracture behavior in small punch test by combined recrystallization-etch method and rigid plastic analysis. J Test Eval 1987;15(1):30–7.

[15] Sih GC, Paris PC, Erdogan F. Crack-tip stress-intensity factors for plane extension and plate bending problems. J Appl Mech 1962; 306–12.

[16] Ju J-B, Kwon D. Assessment of fracture characteristics from revised small punch test using pre-cracked specimen. Metal Mater 1998;4: 742–6.

[17] Foulds JR, Wytowitz PJ, Parnell TK, Jewett CW. Fracture toughness by small punch testing. J Test Eval 1995;23(1):3–10.

[18] ASTM. E1921–97; 1998.

[19] Lee BS, Yang WJ, Huh MJ, Hong JH. Evaluation of the fracture toughness transition characteristics for low alloy steels using precracked Charpy specimens. Proceedings of the 11th conference on mechanical behavior of materials 1997;11:517–23.

[20] Sohn K-S, Lee S. Quantitative analysis of fracture toughness using an in-situ SEM loading stage. J Korean Inst Metal Mater 1995;33: 677–81.

[21] Lee B-W, Jang J-i, Kwon D. Evaluation of fracture toughness using small notched specimens. Mater Sci Eng 2002;A334:207–14.

[22] Broek D. The practical use of fracture mechanics. Netherlands: Kluwer Academic Publishers; 1989.

[23] Fleury E, Ha JS. Small punch tests to estimate the mechanical properties of steels for steam power plant: II. Fracture toughness. Int J Pressure Vessels Piping 1998;75:707–13.